Highly efficient Pd–ZnO catalyst doubly promoted by CNTs and Sc_2O_3 for methanol steam reforming

Lu Yang, Guo-Dong Lin, Hong-Bin Zhang[*],[1]

Department of Chemistry, College of Chemistry and Chemical Engineering, State Key Laboratory of Physical Chemistry for Solid Surfaces and National Engineering Laboratory for Green Chemical Productions of Alcohols-Ethers-Esters, Xiamen University, Xiamen 361005, China

ABSTRACT

A type of Pd–ZnO catalyst doubly promoted by CNTs and Sc_2O_3 for methanol steam reforming (MSR) was developed, and displayed excellent activity and operation stability for the selective formation of H_2 and CO_2. Over a $Pd_{0.15}Zn_1Sc_{0.067}$–10%CNTs catalyst under the reaction conditions of 0.5 MPa and 548 K, the $STY(H_2)$ can maintain stable at the level of 1.56 mol h^{-1} g^{-1} at 75 h after the reaction started, which was 1.7 times that of the corresponding (CNTs and Sc)-free counterpart $Pd_{0.15}Zn_1$. Characterization of the catalyst revealed that the highly conductive CNTs could promote hydrogen spillover from the PdZn/ZnO-sites to the CNTs adsorption-sites, and then combine to form $H_2(a)$, followed by desorbing to $H_2(g)$, which would help increase the rate of a series of surface dehydrogenation reactions in the MSR process. The pronounced modification action of Sc^{3+} may be due to the high solubility of Sc_2O_3 in ZnO lattice. Solution of a small amount of Sc_2O_3 in ZnO lattice resulted in the formation of Schottky defects in the form of cationic vacancies at the surface of ZnO, where the $(PdZn)^0$–Pd^{2+} clusters can be better stabilized through the Pd^{2+} accommodated at the surface vacant cation-sites. This would be conducive to inhibiting the sintering of the catalytically active $(PdZn)^0$ nanoparticles, and thus, markedly prolonging the life of the catalyst.

© 2013 Elsevier B.V. All rights reserved.

1. Introduction

There has been a lot of attention recently on the development of suitable catalysts for steam reforming of methanol (MSR; $CH_3OH + H_2O \rightarrow CO_2 + 3H_2$) [1–10]. Most early studies focused on Cu-based catalysts, which exhibit high activity and selectivity to the formation of CO_2 and H_2 [1–3]. However, they suffer from poor heat and oxidation resistances and fast deactivation at reaction temperatures above 543 K.

On the other hand, novel Pd/ZnO systems [5–9] (as well as Pd/Ga_2O_3 [10]) have attracted increasing attention because of their high selectivity to the formation of CO_2 and H_2 and excellent thermal stability. Iwasa et al. [5] were the first to report that, when supported on ZnO and reduced at temperatures higher than 573 K, Pd displayed high activity and selectivity to form CO_2 and H_2. Extremely low CO selectivity was attributed to the formation of bimetallic PdZn alloy dispersed on the ZnO matrix, which modified the catalytic function of Pd [6–8]. The high MSR performance of the Pd/ZnO catalyst was also reported by Chin et al. [9]. Nevertheless, from the practical viewpoint, the activity, especially operation stability, of the Pd/ZnO or Pd/Ga_2O_3 catalysts can still be improved.

Multi-walled carbon nanotubes (simplified as CNTs in later text), as a novel nano-carbon material, have been drawing a lot of attention for catalysis applications in recent years [11–13]. This kind of nanotube-C possesses several unique features, such as highly graphitized tube-wall, nano-sized channel and sp^2-C-constructed surface [14,15]. They also display high thermal/electrical conductivity, medium to high specific surface areas, and excellent performance for adsorbing hydrogen and promoting hydrogen spillover [15,16], all of which render them full of promise to be a novel catalyst carrier and/or promoter. The catalytic studies conducted so far on CNT-based systems have shown promising results in terms of activity and selectivity [11–13].

In the present work, a type of highly efficient Pd–ZnO catalyst doubly promoted by CNTs and Sc_2O_3 was developed. The catalyst displayed higher activity and operation stability for MSR, compared to the corresponding (CNTs and Sc)-free counterpart. The catalyst was characterized by means of TEM/EDX, XRD, XPS, H_2-TPR and H_2-TPD, and the nature of promoter action by the CNTs and Sc_2O_3 was discussed. The results shed light on the design of practical catalysts for the MSR.

* Corresponding author. Tel.: +86 592 2184591; fax: +86 592 2086116.
  E-mail addresses: zenobiapost@yahoo.com.cn (L. Yang), gdlin@xmu.edu.cn
(G.-D. Lin), hbzhang@xmu.edu.cn (H.-B. Zhang).
  [1] Tel.: +86 592 2181888; fax: +86 592 2081888.

2. Experimental

2.1. Catalyst preparation

The CNTs used in the present work were prepared following the method reported previously [14]. The freshly prepared CNTs were purified with treatment of nitric acid (8 mol/L at 363 K) for 8 h, followed by rinsing with de-ionized water twice, and then drying at 383 K under N_2-atmosphere. Open-ended CNTs with somewhat hydrophilic surface were then obtained. For the purified CNTs, contents of the total carbon and the graphitized carbon were $\geq 99.5\%$ and $\geq 90\%$ (mass%), respectively.

A series of Pd–ZnO or Pd–ZnO–Sc_2O_3 catalysts doped with CNTs, denoted as Pd_iZn_j(or $Pd_iZn_jSc_k$)–$x\%$(mass percentage)CNTs, were prepared by a co-precipitation method. An aqueous solution containing calculated amounts of $PdCl_2$ and $Zn(NO_3)_2 \cdot 6H_2O$ (or as well as $Sc(NO_3)_3 \cdot 6H_2O$) was added dropwise under vigorous stirring into a Pyrex flask containing a certain amount of aqueous Na_2CO_3 solution at 333 K. The addition was adjusted to maintain the pH of the suspension at 9–10. The suspension was continuously stirred for 30 min at 333 K, followed by cooling down to room temperature before filtering. The filtered cake was repeatedly washed with deionized water until the filtrate became neutral in pH. The washed solid was added into a suspension prepared in advance containing calculated amounts of CNTs, followed by stirring vigorously for 4 h, and then centrifuging-filtering. The obtained solid was dried at 383 K for 12 h and calcined at 633 K for 2 h, yielding the precursor of Pd_iZn_j–$x\%$CNTs or $Pd_iZn_jSc_k$–$x\%$CNTs catalysts (in oxidation state).

The CNT-free counterparts were prepared in the similar manner, and used as reference. All samples of catalyst precursor were pressed, crushed, and sieved to a size of 20–40 mesh for the activity evaluation.

2.2. Catalyst evaluation

Activity tests of the catalyst for MSR were carried out in a fixed-bed continuous-flow reactor-GC combination system. Catalyst (0.200 g) was mixed with 4.0 g quartz sand (inert diluents, 20–40 mesh) to order to maintain isothermal conditions, and placed in the reactor. Prior to the reaction, the catalyst was pre-reduced *in situ* under purified H_2 stream (0.1 MPa and 1800 mL h^{-1}). The reduction temperature was programmed to rise from room temperature to 523 K and maintain at that temperature for 12 h, before being brought to the desired temperature for the catalyst test. The MSR reaction was conducted at a stationary state under the reaction conditions of 0.5 MPa and 473–673 K. A pre-mixed feed-liquid of methanol and water (molar ratio of 1:1) was introduced into the reactor by using a syringe pump (Series II Pump, 10 mL Heads). Prior to entering the reactor, the feed-liquid was fully vaporized through a vaporizer, operating at 473 K. N_2 (of 99.99% purity) was used as the dilution gas to maintain the mol% of the pre-mixed CH_3OH–H_2O (molar ratio of 1:1) in the feed-gas ((CH_3OH–H_2O) + N_2) at the desired level (controlled by Model D08-1F flow control valve). The corresponding gas hourly space velocity (*GHSV*) of the feed-gas ranged in 54,000–216,000 mL h^{-1} g^{-1}. A glass condenser at 278 K was used to separate liquid products from gaseous products. The gaseous products were analyzed by an on-line GC (Model GC-2014C, Shimadzu) equipped with a TCD detector and a column filled with carbon molecular sieve (TDX-01, 2.0-m length), which was used for the analysis of N_2 (as internal standard), CO and CO_2. The experimental results showed that CO_2 and CO were the only two carbon-containing products of the MSR reaction, without other possible carbon-containing products detected. Thus, selectivity to CO_2 and CO (symbolized as $S(CO_2)$ and $S(CO)$) could be determined by an internal normalization method, and methanol conversion (noted as $X(CH_3OH)$) and H_2 space-time-yield (noted as

$STY(H_2)$) could be calculated through the yields of CO_2 and CO. All data were taken 24 h after the reaction started (unless otherwise specified).

2.3. Catalyst characterization

Transmission electron microscopy (TEM) and energy-dispersive X-ray spectroscopy (EDX) measurements were performed on JEM-1400 and Hitachi S-4800 electron microscopes, respectively. XRD measurements were carried out on an X'Pert PRO X-ray diffractometer (PANalytical) with Cu Kα ($\lambda_{\alpha 1}$ = 0.15406 nm, $\lambda_{\alpha 2}$ = 0.15443 nm) radiation. A continuous scan mode was used to collect 2θ data from 10° to 90°. The voltage and current were 40 kV and 30 mA, respectively. X-ray photoelectron spectroscopy (XPS) measurements were done on a Quantum 2000 Scanning ESCA Microprobe instrument with Al Kα radiation (15 kV, 25 W, $h\nu$ = 1486.6 eV) under ultrahigh vacuum (5×10^{-7} Pa), calibrated internally by the carbon deposit C($1s$) (E_b = 284.7 eV).

Specific surface area (SSA) was determined by N_2 adsorption using a Micromeritics ASAP 2020 system. Measurement of CO chemisorption on the catalysts was performed by a Micromeritics ASAP-2010 Micropore Analyzer. 0.1–0.2 g of catalyst sample was used for each test. The sample was put into a quartz tube, followed by evacuating for 10 min at 393 K, then switching to a purified H_2 stream (30 mL min^{-1}) as reducing gas to conduct an *in situ* H_2-TPR treatment of the catalyst sample, subsequently evacuating for 1 h at the reduction temperature and another 1 h after cooling down to room temperature, and then switching to gaseous CO (of 99.99% purity) to conduct the CO chemisorption measurement. From the determined amount of chemisorbed CO, the dispersion and surface area of metallic palladium were calculated [17].

Tests of H_2-temperature-programmed reduction (H_2-TPR) of oxidation precursor of the catalysts were conducted on a fixed-bed continuous-flow micro-reactor. A NaOH-column and a 3A-zeolite column were installed in sequence at the reactor-exit to remove water vapor formed by the reduction of metal oxides of the catalyst sample. Fifty mg of catalyst sample was used for each test. The sample was first flushed by an Ar (of 99.999% purity) stream (60 mL min^{-1}) at 393 K for 60 min to clean its surface, and then cooled down to room temperature, followed by switching to a N_2-carried 5 vol% H_2 gaseous mixture as reducing gas to start the TPR observation. The rate of temperature increase was 5 K min^{-1}. Change of hydrogen-signal was monitored by an on-line GC (Shimadzu GC-8A) with a TC detector.

Tests of H_2-temperature-programmed desorption (H_2-TPD) of the catalysts were conducted on an adsorption/desorption system. Two hundred milligram of the catalyst precursor was used in each test. Prior to the H_2-TPD test, the sample of catalyst-precursor was *in situ* pre-reduced in a H_2 (of 99.999% purity) stream (900 mL h^{-1}) at 523 K for 2 h and then flushed by an Ar (of 99.999% purity) stream (1800 mL h^{-1}) at 433 K for 30 min to clean its surface, followed by switching to the H_2 (of 99.999% purity) stream for hydrogen adsorption for 30 min and subsequently at room temperature for 4 h. Afterwards, the sample was flushed by the Ar stream at room temperature until the stable baseline in GC appeared. TPD measurements were then conducted from 298 K to 1073 K. The rate of temperature increase was 5 K min^{-1}. Change of hydrogen-signal was monitored by an on-line GC (Shimadzu GC-8A) with a TC detector.

3. Results and discussion

3.1. Optimization of the catalyst composition

The reactivity of MSR over a series of $Pd_{0.15}Zn_1$–$x\%$CNTs catalysts with varied amounts of CNTs was first
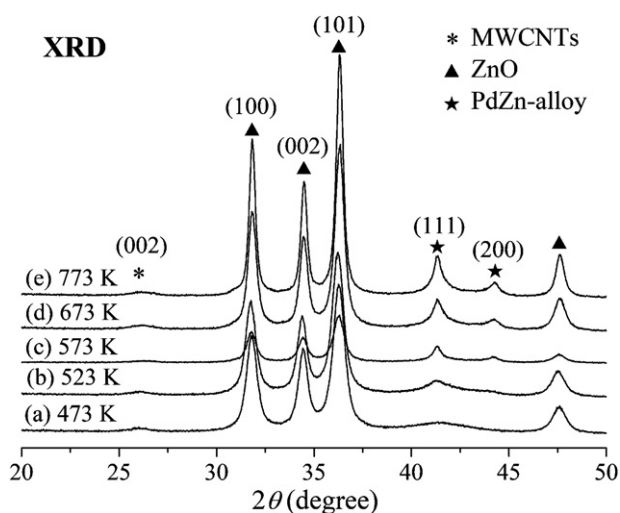
Fig. 1. XRD patterns of the $Pd_{0.15}Zn_1$–x%CNTs catalyst reduced at different temperatures, as indicated in the figure.
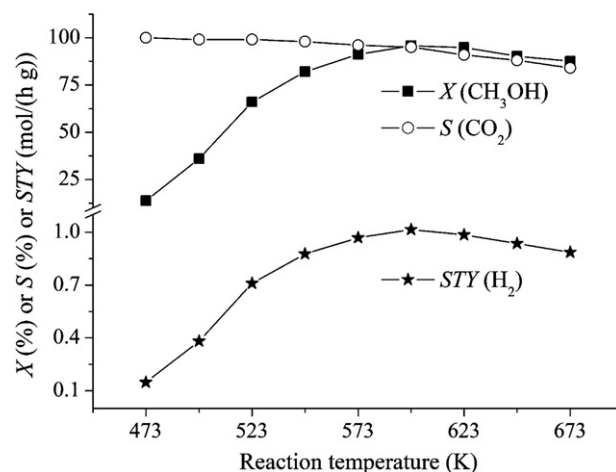

Fig. 2. Reactivity of MSR over the $Pd_{0.15}Zn_1$–10%CNTs catalyst with varying temperatures; the reaction conditions: 0.5 MPa, the feed-gas composition $CH_3OH/H_2O/N_2 = 7.5/7.5/85$ (molar ratio), $GHSV = 108,000$ mL h^{-1} g^{-1}.

investigated. The results show that CO_2 and CO were the only two carbon-containing products observed. Among the five tested catalysts of $Pd_{0.15}Zn_1$–x%CNTs (x% = 5%, 7.5%, 10%, 12.5%, 15%), $Pd_{0.15}Zn_1$–10%CNTs showed the highest activity for MSR. Over this catalyst under the reaction conditions of 0.5 MPa, 523 K, feed-gas composition of $CH_3OH/H_2O/N_2 = 7.5/7.5/85$ (molar ratio) and $GHSV = 108,000$ mL h^{-1} g^{-1}, $X(CH_3OH)$ reached 67.0%, with the corresponding $STY(H_2)$ being 0.72 mol h^{-1} g^{-1}. $X(CH_3OH)$ of the other four catalysts with x% = 5%, 7.5%, 12.5%, 15% was 61.6%, 65.2%, 64.3%, 59%, with the corresponding $STY(H_2)$ being 0.66, 0.70, 0.69, 0.63 mol h^{-1} g^{-1}, successively.

Next, the Pd/Zn molar ratio (i/j) of the Pd_iZn_j-10%CNTs catalysts was optimized. The results showed that the catalyst with i/j = 0.15 displayed the highest activity for MSR. Over the $Pd_{0.15}Zn_1$–10%CNTs catalyst under the aforementioned reaction conditions, $X(CH_3OH)$ reached 67.0%, with the corresponding $STY(H_2)$ being 0.72 mol h^{-1} g^{-1}. $X(CH_3OH)$ of the other four catalysts with i/j = 0.05, 0.10, 0.2, 0.25 was 43.9%, 57.1%, 66.3%, 58.4%, with the corresponding $STY(H_2)$ being 0.47, 0.61, 0.71, 0.63 mol h^{-1} g^{-1}, successively.

3.2. Optimization of the reaction operation conditions

3.2.1. Reduction temperature

The reduction temperature for the precursor of the $Pd_{0.15}Zn_1$–10%CNTs catalyst has a marked effect on the performance of catalyzing MSR. The test results showed that the catalyst reduced by H_2 at 523 K displayed the highest activity for MSR, with $X(CH_3OH)$ and $STY(H_2)$ reaching 67% and 0.72 mol h^{-1} g^{-1} under the aforementioned reaction conditions; while the $X(CH_3OH)$ of the other four catalysts reduced by H_2 at 473 K, 573 K, 673 K and 773 K, respectively, was 61%, 66%, 58% and 38%, with the corresponding $STY(H_2)$ being 0.65, 0.71, 0.62 and 0.41 mol h^{-1} g^{-1}, successively, under the same reaction conditions. Therefore, 523 K is taken as the optimal reduction temperature for this catalyst in order to achieve both high $X(CH_3OH)$ and $STY(H_2)$.

The results of XRD measurement (Fig. 1) provided direct evidence of the formation of PdZn alloy upon the reduction of the CNT-doped Pd–ZnO catalyst. In the XRD patterns taken on the four samples of $Pd_{0.15}Zn_1$–10%CNTs reduced at 523, 573, 673 and 773 K, respectively, the peak at $2\theta = 40.1°$ (originating from the (1 1 1) diffraction of metallic Pd_x^0) completely vanished, while the two peaks at $2\theta = 41.2°$ and 44.1° (due to the (1 1 1) and (2 0 0) diffractions of PdZn alloy, respectively [18]) markedly enhanced,

indicating the formation of PdZn alloy-phase as the predominant Pd-containing crystallite-phase. Using the well-known Scherrer's equation, the average particle size of PdZn-alloy crystallites of the four samples in Fig. 1 was estimated to be: (b) 7.5 nm, (c) 13.7 nm, (d) 16.3 nm, and (e) 19.7 nm, respectively. The upward trend of the particle size of PdZn-alloy crystallites with rising reduction-temperature implied that the sequence of the exposed area of PdZn-alloy in those samples was: (b) > (c) > (d) > (e), in line with the aforementioned observed sequence of catalytic activity of those catalysts for MSR.

As observed by Datye et al. [8] on the Pd–ZnO catalyst reduced at temperatures of <523 K, PdZn alloy and monometallic Pd_x^0 crystallites coexisted in the $Pd_{0.15}Zn_1$–10%CNTs catalyst reduced at 473 K. The average particle size of the former was estimated to be 4.5 nm, while the latter was unable to display the characteristic peak in the corresponding XRD pattern (Fig. 1(a)) probably due to their particle sizes of $\leq$3 nm. Lower-temperature reduction led to incomplete transformation of Pd into the PdZn alloy, therefore resulting in lower activity of the corresponding catalyst for MSR.

The above XRD-analysis results, in connection with above-mentioned those of catalyst assay, demonstrated that the catalytically active phase associated more closely with the MSR was PdZn alloy, rather than metallic Pd, especially under reaction temperatures of $\geq$523 K, in line with the results reported in the previous literatures [6,8].

3.2.2. Reaction temperature

Reaction temperature has a pronounced effect on the conversion of MSR and the selectivity of CO_2 formation. Fig. 2 displayed the reactivity of MSR over the catalyst of $Pd_{0.15}Zn_1$–10%CNTs at varying temperatures. With the reaction temperature rising progressively from 473 K, $X(CH_3OH)$ ascended quickly before reaching a maximum at 598 K, and then slowly descended; while S_{CO_2} descended monotonously. In order to achieve both high $S(CO_2)$ and $X(CH_3OH)$, 548 K was taken as the optimal operating temperature.

3.2.3. Feed-gas GHSV

In order to find out the working conditions with great extent of reaction, the reactivity of MSR over the $Pd_{0.15}Zn_1$–10%CNTs catalyst was tested under a series of reaction conditions with varying $GHSV$ of the feed-gas. The results in Fig. 3 showed that, with $GHSV$ of the feed-gas rising progressively from 54,000 mL h^{-1} g^{-1}, $X(CH_3OH)$ decreased monotonously and $S(CO_2)$ maintained continuously at a high level of ~98%. Meanwhile, $STY(H_2)$ increased in the lower
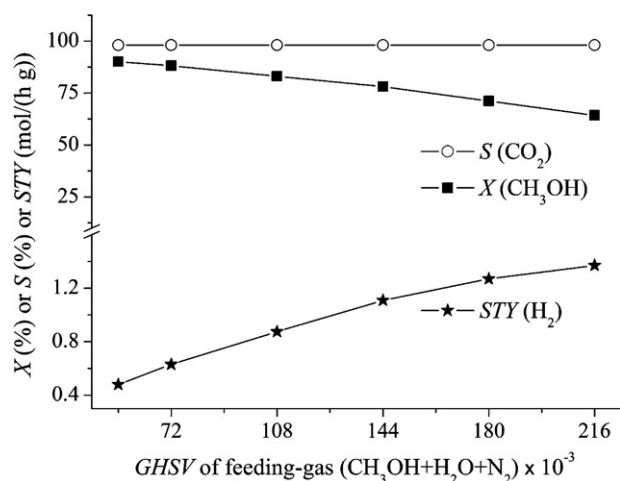
Fig. 3. Reactivity of MSR over the $Pd_{0.15}Zn_1-10\%CNTs$ catalyst with varying *GHSV* of the feed-gas; the reaction conditions: 0.5 MPa, 548 K, the feed-gas composition $CH_3OH/H_2O/N_2 = 7.5/7.5/85$ (molar ratio) and *GHSV* ranging in 56,000–216,000 mL h^{-1} g^{-1}.

Fig. 5. Operating stability of MSR over the catalysts of: (a) $Pd_{0.15}Zn_1Sc_{0.067}-10\%CNTs$; (b) $Pd_{0.15}Zn_1-10\%CNTs$; (c) $Pd_{0.15}Zn_1$; at reaction conditions of 0.5 MPa, 548 K, $CH_3OH/H_2O/N_2 = 30/30/40$ (molar ratio) and *GHSV* = 180,000 mL h^{-1} g^{-1}.

GHSV region, and approached a plateau when the *GHSV* reached 180,000 mL h^{-1} g^{-1} and above. In order to simultaneously achieve relatively high $X(CH_3OH)$ and $S(CO_2)$, as well as $STY(H_2)$, *GHSV* of the feed-gas was set at 180,000 mL h^{-1} g^{-1}.

3.2.4. Feed-gas composition

The composition of feed-gas has a marked effect on the extent of MSR reaction. The MSR reactivity over the $Pd_{0.15}Zn_1-10\%CNTs$ catalyst with varying feed-gas compositions was evaluated. The results in Fig. 4 showed that, with mol% of the pre-mixed CH_3OH-H_2O (molar ratio of 1:1) in the feed-gas ((CH_3OH-H_2O) + N_2) rising progressively from 15% to 75%, $X(CH_3OH)$ decreased monotonously, and $S(CO_2)$ maintained continuously at a high level of 98–96%. Meanwhile, $STY(H_2)$ slowly descended after reaching a maximum at the mol% = 60%. In order to achieve both high $STY(H_2)$ and low consumption of raw-material methanol, (CH_3OH-H_2O):(N_2) = 60:40 (mol/mol) was taken as the optimal composition of feed-gas.
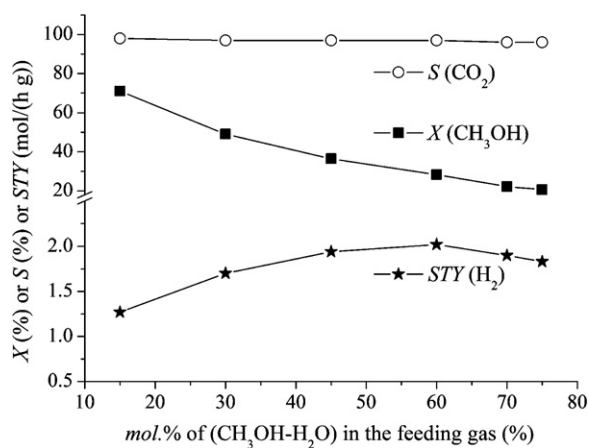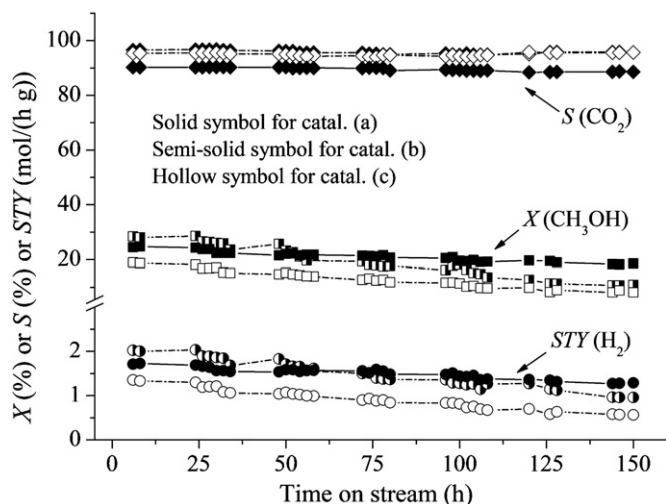

Fig. 4. Reactivity of MSR over the $Pd_{0.15}Zn_1-10\%CNTs$ catalyst with varying mol% of the premixed CH_3OH-H_2O (molar ratio of 1:1) in the feed-gas ((CH_3OH-H_2O) + N_2); at reaction conditions of 0.5 MPa, 548 K, *GHSV* = 180,000 mL h^{-1} g^{-1} and the mol% of the pre-mixed CH_3OH-H_2O in the feed-gas ranging in 15–75%.

3.3. Performance of CNT-promoted $Pd_{0.15}Zn_1$-based catalysts and reference system for MSR

In order to evaluate the performance of the CNT-promoted Pd–ZnO based catalysts under the working conditions with great extent of reaction, the MSR reaction was conducted under the aforementioned optimized reaction conditions: 0.5 MPa, 548 K, feed-gas composition $CH_3OH/H_2O/N_2 = 30/30/40$ (molar ratio) and *GHSV* = 180,000 mL h^{-1} g^{-1}. Table 1 lists the results taken at 75 h after the reaction started. Over the $Pd_{0.15}Zn_1-10\%CNTs$ catalyst, $X(CH_3OH)$ reached 19.3%, with the corresponding $STY(H_2)$ being 1.50 mol h^{-1} g^{-1}. This $STY(H_2)$ value was 1.67 times that of the corresponding CNT-free counterpart, $Pd_{0.15}Zn_1$.

Fig. 5(b) and (c) shows the operation stability of the $Pd_{0.15}Zn_1-10\%CNTs$ catalyst and the corresponding CNT-free counterpart for the MSR lasting 150 h. Over the two catalysts, throughout the reaction, $S(CO_2)$ maintained stable at the level of ~95%, while $X(CH_3OH)$ and $STY(H_2)$ descended gradually, and came down to 10.8% and 0.96 mol h^{-1} g^{-1} for the former, and 8.1% and 0.56 mol h^{-1} g^{-1} for the latter, after 150 h of reaction.

We observe that doping an appropriate amount of Sc_2O_3 into the Pd–ZnO based catalysts can significantly improve their operation stability for the MSR. The activity of three catalysts of $Pd_{0.15}Zn_1Sc_k$-10%CNTs with $k = 0.05, 0.067, 0.1$ for the MSR was evaluated. The results showed that the catalyst with $k = 0.067$ displayed the optimal activity and operating stability. Over this catalyst under the reaction condition of 0.5 MPa, 548 K, $CH_3OH/H_2O/N_2 = 30/30/40$ (molar ratio) and *GHSV* = 180,000 mL h^{-1} g^{-1}, $X(CH_3OH)$ reached 21.4% at 75 h after the reaction started, with the corresponding $STY(H_2)$ being 1.56 mol h^{-1} g^{-1} (see Table 1). Meanwhile over the other two catalysts with $k = 0.05, 0.1$, $X(CH_3OH)$ was 18.9% and 12.6%, respectively, with the corresponding $STY(H_2)$ being 1.31 and 0.91 mol h^{-1} g^{-1}, under the same reaction conditions.

Fig. 5(a) showed the operating stability of the $Pd_{0.15}Zn_1Sc_{0.067}-10\%CNTs$ catalyst for MSR lasting 150 h. After around 24 h of "running in" stage of the reaction, the catalyst reached a stable operating state, and after 150 h of reaction, $STY(H_2)$ maintained stable at the level of 1.29 mol h^{-1} g^{-1}, with no sign of obvious deactivation observed.

The apparent activation energy (E_a) of the MSR reaction over the three catalysts tested was measured under the reaction conditions with mass transfer limitation ruled out.

Table 1
Reactivity of MSR over the CNTs and Sc_2O_3 doubly promoted Pd–ZnO catalyst and the reference systems.[a]

Catalyst	Specific surface area (m^2/g)	Mean pore diameter (nm)	PdZn-alloy SA (m^2/g)	$X(CH_3OH)$ (%)	Selectivity of C-containing products (%)		$STY(H_2)$ $(mol\,h^{-1}\,g^{-1})$
					$S(CO_2)$	$S(CO)$	
$Pd_{0.15}Zn_1$	82.3	11.2	27.0	12.7	94.4	5.6	0.90
$Pd_{0.15}Zn_1$–10%CNTs	75.0	11.5	26.8	19.3	95.6	4.4	1.50
$Pd_{0.15}Zn_1Sc_{0.067}$–10%CNTs	100.6	10.9	31.5	21.4	90.0	10.0	1.56

[a] The reaction conditions: 0.5 MPa, 548 K, the feeding-gas composition $CH_3OH/H_2O/N_2$ = 30/30/40 (molar ratio), $GHSV$ = 180,000 mL h^{-1} g^{-1}; the data were taken 75 h after the reaction started.

The results showed that the E_a of MSR reaction observed on the three catalysts, $Pd_{0.15}Zn_1$, $Pd_{0.15}Zn_1$–10%CNTs and $Pd_{0.15}Zn_1Sc_{0.067}$–10%CNTs, was 87.8, 86.4 and 86.2 kJ mol^{-1}, respectively, under the reaction conditions of 0.5 MPa, 473–573 K, feed-gas composition $CH_3OH/H_2O/N_2$ = 30/30/40 (molar ratio) and $GHSV$ = 432,000 mL h^{-1} g^{-1}. These E_a values were fairly close to each other, indicating that appropriate incorporation of a minor amount of either simple CNTs or CNTs and Sc_2O_3 into the $Pd_{0.15}Zn_1$ host catalyst did not cause a marked change in the E_a for the MSR reaction, implying that such doping did not alter the major reaction pathway of steam reforming of CH_3OH to yield H_2 and CO_2.

3.4. Characterization of the catalysts

3.4.1. TEM and EDX characterization
Fig. 6(a) showed the TEM image of the CNTs used in the present work. Previous studies [14,15] have demonstrated that this type of CNTs was a "Herringbone-type" of CNTs, with the outer diameters of 10–50 nm, inner diameters of 3–8 nm, and N_2-BET surface area of ~125 m^2/g. Fig. 6(b)–(d) showed the TEM images of the three used catalysts of $Pd_{0.15}Zn_1$, $Pd_{0.15}Zn_1$–10%CNTs and $Pd_{0.15}Zn_1Sc_{0.067}$–10%CNTs, respectively, from which the particle size of the PdZn-alloy crystallites was estimated to be 12–16 nm, 10–16 nm and 4–7 nm, respectively. The results of the corresponding EDX measurement showed that the element compositions of the surface of the three used catalysts were: Pd/Zn/O = 6.4/38.7/54.9 (mol%) for the $Pd_{0.15}Zn_1$, Pd/Zn/O/C = 4.0/28.9/39.2/27.9 (mol%) for the $Pd_{0.15}Zn_1$–10%CNTs, and Pd/Zn/O/C/Sc = 3.7/24.6/44.4/26.7/0.6 (mol%) for the $Pd_{0.15}Zn_1Sc_{0.067}$–10%CNTs. This result indicated that the doping a minor amount of Sc_2O_3 into the $Pd_{0.15}Zn_1$–10%CNTs catalyst led to an increase by an appreciable amount in mol% of oxygen at the quasi-functioning surface of the used $Pd_{0.15}Zn_1Sc_{0.067}$–10%CNTs catalyst, implying an obvious decrease of mol% of the Pd reduced to Pd^0 in the total surface Pd amounts.
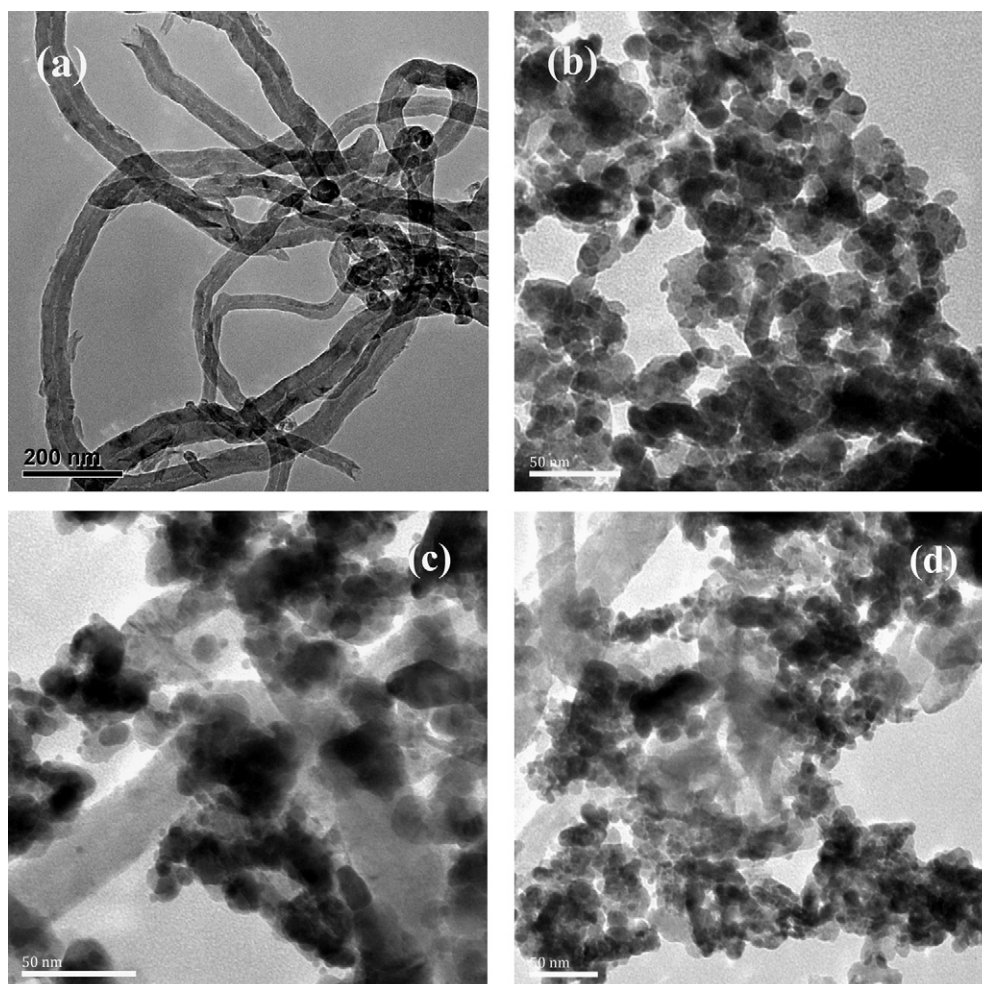

Fig. 6. TEM images of: (a) CNTs; (b) the used $Pd_{0.15}Zn_1$; (c) the used $Pd_{0.15}Zn_1$–10%CNTs; (d) the used $Pd_{0.15}Zn_1Sc_{0.067}$–10%CNTs.
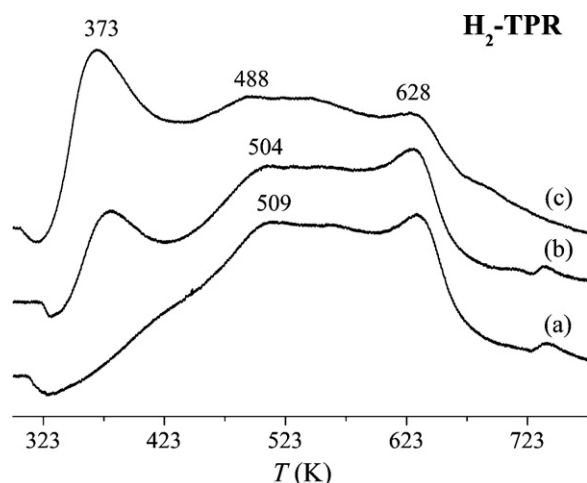
Fig. 7. TPR profiles of the catalyst precursors in oxidation state by H_2: (a) $Pd_{0.15}Zn_1$ ($\times 90\%$); (b) $Pd_{0.15}Zn_1$–10%CNTs; (c) $Pd_{0.15}Zn_1Sc_{0.067}$–10%CNTs.

Fig. 8. XRD patterns of the used catalysts: (a) $Pd_{0.15}Zn_1$; (b) $Pd_{0.15}Zn_1$–10%CNTs; (c) $Pd_{0.15}Zn_1Sc_{0.067}$–10%CNTs.

3.4.2. H_2-TPR test of catalysts in oxidation state

H_2-TPR of the catalyst provided useful information about the reducibility of catalyst. Fig. 7 showed the H_2-TPR profiles taken on the three catalysts in oxidation-state. The H_2-reduction of the $Pd_{0.15}Zn_1$ catalyst (Fig. 7(a)) started at ~323 K and the main TPR-peaks appeared at 509 K and 628 K. The lower-temperature reduction peak (spanning from 323 K to 509 K) may be ascribed to the continuous multi-step single-electron reduction of a large portion of Pd^{n+} species, while the higher-temperature peak (628 K) likely included the contribution from the reduction of the Zn^{2+} species near the Pd_x^0 to form PdZn alloy, in addition to that of the subsequent reduction of the remaining Pd^{n+} species, which were difficult to be reduced at the lower temperatures. Interestingly, the doping of CNTs resulted in the appearance of a new peak at ~373 K, in addition to the 509-K peak downshifting to 504 K or 488 K (see Fig. 7(b) and (c) *vs.* (a)).

The specific H_2-consumed amounts (*i.e.*, the amount of hydrogen consumed due to reduction of unit mass of Pd) of the three catalysts in the region of 323–673 K were estimated, and the obtained relative ratio was: $S_{(a)}/S_{(b)}/S_{(c)} = 90.6/93.8/100$. The higher specific H_2-consumed amount indicated the higher percentage of the Pd^{n+} species reducible to lower valence in the total Pd amount. Based upon the difference in the specific H_2-consumed amounts and the position (*i.e.* reduction temperature) of the corresponding main H_2-reduction peaks, it could be inferred that the sequence of reducibility of the three catalysts was as follows: $Pd_{0.15}Zn_1 < Pd_{0.15}Zn_1$–10%CNTs $< Pd_{0.15}Zn_1Sc_{0.067}$–10%CNTs. Conceivably, the lower reduction-temperature would be beneficial to inhibiting the aggregation of PdZn-alloy crystallites formed by H_2-reduction, thus favorable to increasing the Pd^0(PdZn-alloy) exposed area (see Table 1), and subsequently, improving the catalytic activity for MSR.

3.4.3. Post-reaction analysis of the used catalysts by XRD and XPS

The XRD post-reaction analysis (Fig. 8) showed that there were few differences among the three used catalysts in their XRD features related with the Pd and Zn components, except the feature at $2\theta = 26.1°$ for the CNT-containing systems, which was due to the diffraction of (0 0 2) plane of graphite-like tube-wall of the CNTs [15]. In these used catalysts, the Pd and Zn components existed mainly in the forms of ZnO and PdZn alloy (with the observed XRD features at $2\theta = 31.8°/34.5°/36.3°/47.6°$ and $41.2°/44.1°$, respectively) [18]. The XRD feature at $2\theta = 40.1°$ (due to the diffraction of (1 1 1) plane of metallic Pd_x^0 crystallites [18]) was not detected, suggesting that the content of metallic Pd_x^0-phase was below the
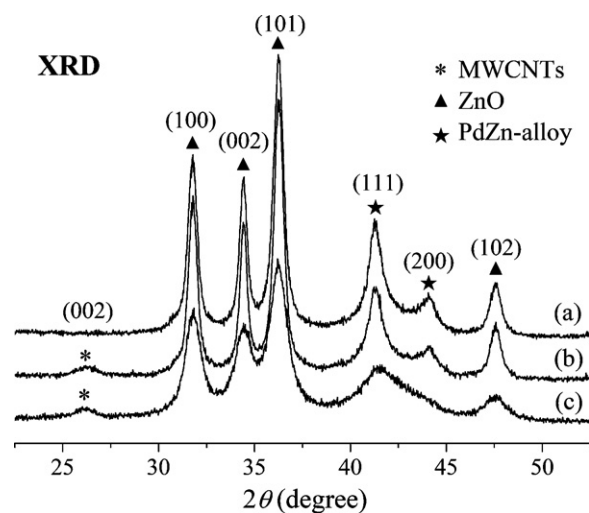
XRD-detection limit. Using the Scherrer's equation, the PdZn-alloy particle size for the three used catalysts was estimated. The calculated average particle size of the PdZn-alloy crystallites was 14.1 nm, 12.5 nm and 4.5 nm, for $Pd_{0.15}Zn_1$, $Pd_{0.15}Zn_1$–10%CNTs and $Pd_{0.15}Zn_1Sc_{0.067}$–10%CNTs, respectively, very close to those estimated from the corresponding TEM images (Fig. 6(b)–(d)). This result showed an upward trend of PdZn-alloy dispersity with the addition of small amounts of Sc^{3+}.

XPS-analysis of the used catalysts revealed that certain difference existed among the three catalysts in the valence-states of the surface Pd species and their relative concentration. Fig. 9 displayed the Pd(3d)-XPS spectra taken on the three used catalysts. The observed $Pd(3d_{5/2})$ and $(3d_{3/2})$ XPS peaks appeared at ~335.6 and ~340.9 eV. These values are characteristic of Pd-species with mixed valences. According to Ref. [19] and through computer-fitting, it could be found that each of those Pd(3d)-XPS spectra involved the contribution from two or three types of surface Pd-species: Pd^0(PdZn-alloy) and Pd^{2+}(PdO), as well as Pd^{4+}(PdO$_2$), with the *B.E.* value of $Pd^0(3d_{5/2, 3/2})$, $Pd^{2+}(3d_{5/2, 3/2})$ and $Pd^{4+}(3d_{5/2, 3/2})$
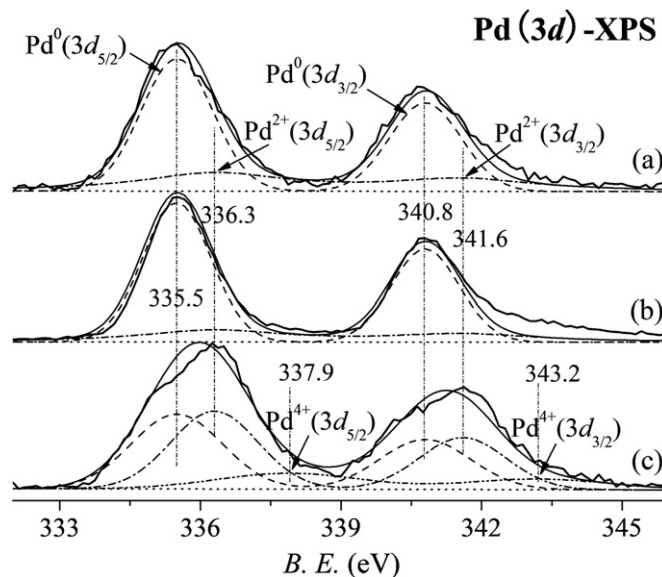

Fig. 9. XPS spectra of Pd(3d) of the used catalysts: (a) $Pd_{0.15}Zn_1$; (b) $Pd_{0.15}Zn_1$–10%CNTs; (c) $Pd_{0.15}Zn_1Sc_{0.067}$–10%CNTs.

being 335.5/340.8 eV, 336.3/341.6 eV and 337.9/343.2 eV, respectively (see Fig. 9). At the quasi-functioning surface of the used $Pd_{0.15}Zn_1$–10%CNTs catalyst (Fig. 9(b)), the mol% of Pd^0-species in the total surface Pd-amount reached 79.9%. This value was higher than that (71.8 mol%) of the CNTs-free host catalyst, $Pd_{0.15}Zn_1$ (Fig. 9(a)), suggesting that the addition of an appropriate amount of CNTs to the host catalyst improve the reducibility of the catalyst, resulting in the increase of the mol% of Pd^0-species in the total surface Pd-amount.

Iwasa et al. [5] were the first to report that the catalytic performance of Pd/ZnO in MSR is greatly improved by previously reducing the catalyst at higher temperatures. Afterwards, Datye et al. [8] found that PdZn alloy particles could be formed after reaction at 523 K, due to the facile reduction of ZnO in the presence of Pd and H_2. Currently, it is well acknowledged that the original catalytic functions of metallic Pd are modified by the formation of PdZn alloys upon the reduction of the Pd/ZnO [6–8]. The present XRD and XPS analysis results, combined with the results of the aforementioned catalyst tests (Table 1), once again confirmed that there existed close correlation between the surface Pd^0-species in form of PdZn alloys and the excellent selectivity for MSR. The high concentration of the surface Pd^0-species in the form of PdZn alloys was conducive to the selective formation of H_2 and CO_2 in MSR.

Unlike the case of adding CNTs, the doping of small amounts of Sc^{3+} into the catalyst system significantly enhanced the mol% of Pd^{2+}(as well as Pd^{4+})-species (with the mol% of Pd^{2+}- and Pd^{4+}-species ascending to 42.7% and 14.4%, respectively, correspondingly with the mol% of Pd^0-species descending to 42.9%) at the catalyst surface (see Fig. 9(c)). The pronounced modification action of Sc^{3+} may be due to high solubility of Sc_2O_3 in ZnO lattice, as the ionic radius of Sc^{3+} (0.0745 nm) is close to that of Zn^{2+} (0.074 nm). Solution of a small amount of Sc_2O_3 in ZnO lattice will result in the formation of cationic vacancies unless it is compensated by solution of an equivalent amount of Pd^+. Yet Pd^+ is not stable and apparently does not dissolve appreciably in ZnO lattice because of the much larger ionic radius (known $r(Pd^{2+})$ = 0.085 nm). Thus the Schottky defects in the form of cationic vacancies due to dissolved Sc_2O_3 in ZnO lattice will diffuse to the ZnO surface, where $(PdZn)^0$–Pd^{n+} (n = 1 or 2) clusters can be better stabilized through the Pd^{n+} accommodated at the surface vacant cation-sites to achieve valence and charge compensation for subsurface layers of Sc^{3+}-doped ZnO. This would be conducive to inhibiting removal and sintering of the catalytically active $(PdZn)^0$ nanoparticles, and thus, markedly prolonging the life of the catalyst (see Fig. 5(a)).

3.4.4. H_2-TPD test of hydrogen adsorption on pre-reduced catalysts

The previous TPD investigation [16] of H_2/CNTs adsorption system showed that hydrogen adsorption on the CNTs can occur at ambient temperatures, and that H_2 adsorption on the CNTs may occur in two forms: associative (molecular state) and dissociative (atomic state), which had been previously confirmed by laser Raman spectroscopy characterization of the H_2/CNTs adsorption system [15].

Fig. 10 showed the H_2-TPD profiles of hydrogen adsorbed on the three pre-reduced catalysts. Overall, each profile contained a lower-temperature peak centered at ~353 K and a higher-temperature peak at ~748 K (spanning from 473 to 823 K). The lower-temperature peaks resulted from the desorption of weakly adsorbed H-species, most probably the molecularly adsorbed hydrogen $H_2(a)$, while the higher-temperature peaks may be attributed to the desorption of strongly adsorbed H-species, perhaps the dissociatively adsorbed hydrogen H(a). It is conceivable that in the reaction-temperature region for MSR ($\geq$473 K for the present work), the surface concentration of H-adspecies associated with the 298–473 K region (region-I) was very low, and most of
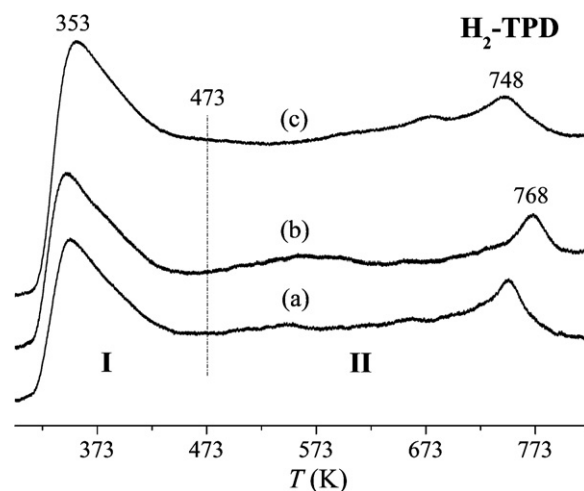

Fig. 10. TPD profiles of H_2 adsorption on the pre-reduced catalysts: (a) $Pd_{0.15}Zn_1$; (b) $Pd_{0.15}Zn_1$–10%CNTs; (c) $Pd_{0.15}Zn_1Sc_{0.067}$–10%CNTs.

H-adspecies at the surface of functioning catalysts was those corresponding to the 473–823 K region (region-II), suggesting that it was those H-adsorption-sites that were closely associated with the reactivity for MSR.

In the MSR process catalyzed by CNT-promoted PdZn/ZnO, the H(a) generated from dehydrogenation of CH_3OH (as well as the intermediate products, HCHO and HCOOH) may *in situ* transfer to the H-adsorption-sites at the CNTs surface, since the highly conductive CNTs might promote hydrogen spillover from the PdZn/ZnO-sites to the adsorption-sites of CNT-surface, combine to form $H_2(a)$ and then desorb to $H_2(g)$, a scenario similar to the case of $Cu_{10}Cr_1$/CNTs-catalyzed deep dehydrogenation of CH_3OH to form H_2 and CO [12,20]. This would be favorable to increasing the rate of a series of surface dehydrogenation reactions in the MSR process. The ratio of relative area-intensities of H_2-TPD profiles in the region-II for those catalysts was estimated to be: $S_{(a)}/S_{(b)}/S_{(c)}$ = 47/56/100. This implied that the sequence of increasing H-adsorption sites at the functioning surface of those catalysts was: $Pd_{0.15}Zn_1$ < $Pd_{0.15}Zn_1$–10%CNTs < $Pd_{0.15}Zn_1Sc_{0.067}$–10%CNTs, in line with the observed sequence of reactivity for MSR on those catalysts.

4. Concluding remarks

(1) A type of highly efficient Pd–ZnO catalysts doubly promoted by CNTs and Sc_2O_3 for MSR was developed.

(2) The CNTs could act as a novel promoter of the Pd–ZnO based catalyst for MSR. The highly conductive CNTs might promote hydrogen spillover from the PdZn/ZnO-sites to the CNTs adsorption-sites. The H(a) generated from dehydrogenation of CH_3OH (as well as the intermediate products, HCHO and HCOOH) may *in situ* transfer to the surface adsorption-sites of CNTs, and combine to form $H_2(a)$ and then desorb to $H_2(g)$, which would be favorable to increasing the rate of a series of surface dehydrogenation reactions in the MSR process.

(3) Sc_2O_3 could act as a novel modifier of the Pd–ZnO based catalyst for MSR. Solution of a small amount of Sc_2O_3 in ZnO lattice resulted in the formation of Schottky defects in form of cationic vacancies at the surface of ZnO, where the $(PdZn)^0$–Pd^{n+} clusters can be better stabilized through the Pd^{n+} accommodated at the surface vacant cation-sites. This would be conducive to inhibiting removal and sintering of the catalytically active $(PdZn)^0$ nanoparticles.

Acknowledgements

Appendix A. Supplementary data

Supplementary data associated with this article can be found, in the online version, at http://dx.doi.org/10.1016/j.apcata. 2013.01.039.

References

[1] A.P. Tsai, M. Yoshimura, Appl. Catal. A: Gen. 214 (2001) 237–241.
[2] Y. Liu, T. Hayakawa, K. Suzuki, S. Hamakawa, T. Tsunoda, T. Ishii, M. Kumagai, Appl. Catal. A: Gen. 223 (2002) 137–145.
[3] X.R. Zhang, P. Shi, J. Zhao, M. Zhao, C. Liu, Fuel Process. Technol. 83 (2003) 183–192.
[4] S.R. Segal, K.B. Anderson, K.A. Carrado, C.L. Marshall, Appl. Catal. A: Gen. 231 (2002) 215–226.
[5] N. Iwasa, S. Kudo, H. Takahashi, S. Masuda, N. Takezawa, Catal. Lett. 19 (1993) 211–216.
[6] N. Iwasa, S. Masuda, N. Ogawa, N. Takezawa, Appl. Catal. A: Gen. 125 (1995) 145–157.
[7] Y. Suwa, S. Ito, S. Kameoka, K. Tomishige, K. Kunimori, Appl. Catal. A: Gen. 267 (2004) 9–16.
[8] A. Karim, T. Conant, A. Datye, J. Catal. 243 (2006) 420–427.
[9] Y.H. Chin, R. Dagle, J. Hu, A.C. Dohnalkova, Y. Wang, Catal. Today 77 (2002) 79–88.
[10] H. Lorenz, S. Penner, W. Jochum, C. Rameshan, B. Klötzer, Appl. Catal. A: Gen. 358 (2009) 203–210.
[11] P. Serp, M. Corrias, P. Kalck, Appl. Catal. A: Gen. 253 (2003) 337–358.
[12] H.B. Zhang, G.D. Lin, Y.Z. Yuan, Curr. Topics Catal. 4 (2005) 1–21.
[13] H.B. Zhang, X.L. Liang, X. Dong, H.Y. Li, G.D. Lin, Catal. Surv. Asia 13 (2009) 41–58.
[14] P. Chen, H.B. Zhang, G.D. Lin, Q. Hong, K.R. Tsai, Carbon 35 (1997) 1495–1501.
[15] H.B. Zhang, G.D. Lin, Z.H. Zhou, X. Dong, T. Chen, Carbon 40 (2002) 2429–2436.
[16] Z.H. Zhou, X.M. Wu, Y. Wang, G.D. Lin, H.B. Zhang, Acta Phys. Chim. Sin. 18 (2002) 692–698.
[17] P.A. Webb, C. Orr, Analytical Methods in Fine Particle Technology, Micromeritics Instrument Co., Norcross, GA, USA, 1997.
[18] XRD Data Bank Attached to X'Pert PRO X-ray Diffractometer (PANalytical, The Netherlands), 2003.
[19] J.F. Moulder, W.F. Stickle, P.E. Sobol, K.D. Bomben, Handbook of X-ray Photoelectron Spectroscopy – A Reference Book of Standard Spectra for Identification and Interpretation of XPS Data, Physical Electronics Inc., Eden Prairie, 1995.
[20] H.B. Zhang, X. Dong, Y.Z. Yuan, G.D. Lin, K.M. Dong, K.R. Tsai, pp. 2–156, 267–268 13th ICC (Paris, 2004) Book of Abstract 1, 2004.